
Detecting Model Misspecification in Amortized Bayesian Inference with Neural Networks

Marvin Schmitt

Cluster of Excellence SimTech
University of Stuttgart, Germany
mail.marvinschmitt@gmail.com

Paul-Christian Bürkner

Cluster of Excellence SimTech
University of Stuttgart, Germany
paul.buerkner@gmail.com

Ullrich Köthe

Computer Vision and Learning Lab, IWR
University of Heidelberg, Germany
ullrich.koethe@iwr.uni-heidelberg.de

Stefan T. Radev

Cluster of Excellence STRUCTURES
University of Heidelberg, Germany
stefan.radev93@gmail.com

Abstract

Recent advances in probabilistic deep learning enable amortized Bayesian inference in settings where the likelihood function is implicitly defined by a simulation program. But how faithful is such inference when simulations represent reality somewhat inaccurately? In this paper, we conceptualize the types of model misspecification arising in simulation-based inference, systematically investigate the performance of SNPE-C (APT) and the BayesFlow framework under these misspecifications and devise a “misspecification alarm”, namely a statistical test signaling suspicious inputs. Our main insight is that this test works most reliably on the level of learnable data summary statistics. Thus, we augment the training objectives to impose probabilistic structure on our models’ latent summary space, so that outlying summaries can be detected by maximum mean discrepancy (MMD). We verify the alarm for various synthetic and real misspecifications and show that outlying summary statistics are powerful proxies for posterior inference errors arising from misspecified simulations, which cannot be identified directly because the true generative process is generally unknown.

1 Introduction

Computer simulations play a fundamental role in many fields of science. However, finding simulation parameters that faithfully reproduce or predict real-world behavior is difficult and usually analytically intractable. Here, we consider *simulation-based inference* (SBI) as a general approach to overcome this difficulty. We conduct analyses of the SNPE-C (APT; Greenberg et al., 2019) and BayesFlow frameworks (Radev et al., 2020a), which utilize deep learning to infer posterior probabilities for the simulation parameters of interest. Specifically, we study how amortized simulation-based inference performs under well-specified vs. misspecified simulations (i. e., simulations that do or do not precisely capture the mechanisms of the real system) and propose a new misspecification measure that reliably detects when the system behavior at test time deviates from the behavior during training. Detecting such deviations is of crucial importance because mild or sometimes severe mismatch between simulated and actual behavior occurs almost inevitably in practice. To this end, we develop a theoretical basis for misspecification detection, incorporate it into simulation-based inference frameworks with learned summary statistics, and investigate it on toy examples and two representative scientific tasks in cognitive decision making and disease outbreak dynamics.

So far, work on deep amortized SBI has mainly focused on finding network architectures and training algorithms that achieve the highest performance (Greenberg et al., 2019; Radev et al., 2020a; Durkan et al., 2020; Lueckmann et al., 2017). In contrast, the consequences of *model misspecification* have received little attention in the context of *amortized* SBI. Model misspecification occurs when a model does not fully represent the actual behavior of the modeled system or when it does not completely account for measurement errors and contamination in the observations serving as inference inputs. In the context of SBI, this is also referred to as a *simulation gap*, and we use the terms interchangeably.

Amortized Bayesian methods require simulations to be faithful proxies of reality and might yield *wrong posteriors* when presented with observables which are atypical under the assumed model (cf. Figure 1). Our experiments clearly demonstrate this effect and show how amortized posterior inference gradually deteriorates as the simulation gap widens. Consequently, amortized SBI methods must be able to detect simulation gaps and subsequent posterior errors, so that they can warn users about suspicious outputs (or even decline to make predictions under such circumstances) and guide model designers in their search for better simulators.

The main purpose of this paper is twofold. First, we conceptualize model misspecification in applications of simulation-based Bayesian inference with neural networks (section 3.1). We then propose a simple and intuitive way to detect model misspecification and posterior inference errors (posterior errors, for short) arising due to finite training (section 3.5). See Figure 1 for a conceptual illustration. Our approach does not modify existing neural architectures and greatly benefits from the properties of amortized inference. Instead, it acts as a modular and intuitive extension of previous work on sequential neural density estimators (SNPE-C; Greenberg et al., 2019), invertible neural networks (INNs; Ardizzone et al., 2018), and the BayesFlow framework (Radev et al., 2020a) towards a principled simulation-based Bayesian workflow. Indeed, the demand for a trustworthy workflow in amortized Bayesian inference increases heavily due to the growing number of applications relying on amortized simulation-based inference (e.g., Shiono, 2021; Bieringer et al., 2021; Dehning et al., 2020; Gonçalves et al., 2020). The key contributions of our paper are:

- (i) A way to conceptualize different sources of model misspecification in amortized Bayesian inference with neural networks;
- (ii) An augmented optimization objective and a criterion to detect model misspecification and posterior errors during inference, regardless of a model’s structure, input, or output;
- (iii) A systematic investigation of our detection criterion and its relationship with posterior errors in a variety of models and misspecifications.

2 Related work

Neural approaches to amortized simulation-based inference can be categorized as either targeting the posterior (Radev et al., 2020a; Greenberg et al., 2019), the likelihood (Papamakarios et al., 2019; Hermans et al., 2020), or both (Wiqvist et al., 2021). We hypothesize that the estimation quality of these approaches will be, in general, unpredictable, when faced with atypical real-world data.

On the other hand, model misspecification has been studied in the context of standard Bayesian inference and various ideas have been explored (Grünwald et al., 2017; Thomas and Corander, 2019). For instance, likelihood tempering methods incorporate a modified likelihood (raised to a power $0 < t < 1$) in order to prevent potentially overconfident Bayesian updating (Thomas and Corander, 2019). However, the likelihood in SBI is assumed to be unknown and thus impossible to evaluate explicitly. Applying likelihood tempering methods to amortized neural likelihoods appears to be another avenue for future research.

For robust non-amortized ABC samplers, the possibility of utilizing hand-crafted summary statistics as an important element of misspecification analysis has already been explored (Frazier et al., 2020; Frazier and Drovandi, 2021). Our work parallels these ideas and extends them to the case of *learnable summary statistics* in amortized SBI on potentially massive data sets, where ABC becomes infeasible. Furthermore, we offer a conceptual discussion on the sources of misspecifications (and their consequences) arising in SBI and explore the connection between posterior errors and model misspecification as a function of the number of summary statistics. In the field of variational Bayes, recent work has studied the convergence and concentration rates with and without misspecification (Alquier and Ridgway, 2019; Zhang and Gao, 2020). These approaches are not directly transferable

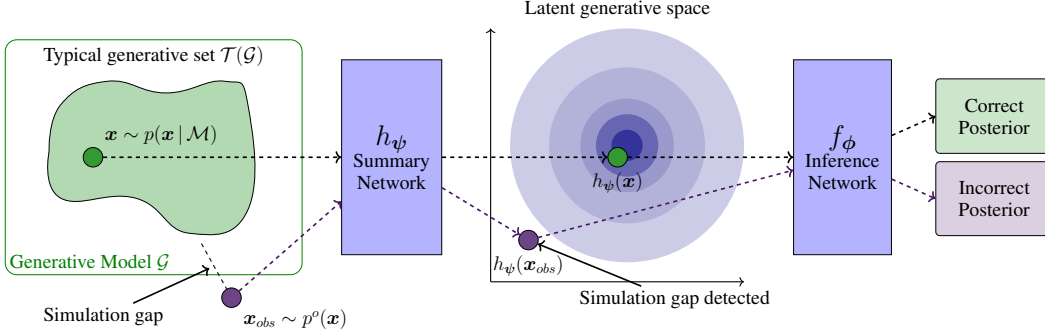


Figure 1: Conceptual overview of our framework as a step towards trustworthy simulation-based inference with neural density estimators. A summary network h_{ψ} transforms the typical generative set $\mathcal{T}(\mathcal{G})$ of a complex model \mathcal{G} into the typical set of a simple distribution (e. g., Gaussian). Simulation gaps between the model-implied distribution of observables $p(\mathbf{x} | \mathcal{M})$ and the one implied by reality $p^o(\mathbf{x})$ manifest themselves as detectable anomalies, causing posterior errors by the inference network f_{ϕ} . These anomalies are flagged by h_{ψ} via distribution matching (maximum mean discrepancy).

to amortized models because they do not naturally provide a practical “misspecification alarm”, which is needed because neural networks remain unchanged after the training phase in SBI.

From the perspective of Bayesian model comparison as classification, different outlier detection techniques appear to be viable for uncovering simulation gaps. For instance, [Radev et al. \(2021a\)](#) propose to train regularized evidential networks which learn a higher-order distribution over posterior model probabilities. This way, conclusions about the absolute misfit of all models in a set of candidate models can be drawn. However, this approach is not suitable for parameter estimation and requires a loss function which does not guarantee a correct approximation of posterior model probabilities.

3 Methods

3.1 Defining model misspecification

For the purpose of simulation-based inference, we define a generative model as a triple $\mathcal{G} = (g(\boldsymbol{\theta}, \boldsymbol{\xi}), p(\boldsymbol{\xi} | \boldsymbol{\theta}), p(\boldsymbol{\theta}))$. Such a model generates data points $\mathbf{x} \in \mathcal{X}$ according to the system

$$\mathbf{x} = g(\boldsymbol{\theta}, \boldsymbol{\xi}) \quad \text{with} \quad \boldsymbol{\xi} \sim p(\boldsymbol{\xi} | \boldsymbol{\theta}), \boldsymbol{\theta} \sim p(\boldsymbol{\theta}), \quad (1)$$

where g denotes a (randomized) simulation program, $\boldsymbol{\xi} \in \Xi$ is a source of randomness (i. e., noise) with density function $p(\boldsymbol{\xi} | \boldsymbol{\theta})$, and $p(\boldsymbol{\theta})$ encodes prior knowledge about plausible simulation parameters $\boldsymbol{\theta} \in \Theta$. Intuitively, \mathbf{x} represents quantities that we can observe and measure in the real-world, $\boldsymbol{\theta}$ consists of hidden properties whose role in g we explicitly understand and model, and $\boldsymbol{\xi}$ takes care of nuisance effects that we only treat statistically. The abstract spaces \mathcal{X} , Ξ , and Θ denote the domain of possible output data (possible worlds), the scope of noise, and the set of admissible model parameters, respectively. The distinction between hidden properties $\boldsymbol{\theta}$ and noise $\boldsymbol{\xi}$ is not entirely clear-cut, but depends on our modeling goals and may vary across applications. Moreover, our understanding of the world is constantly evolving, and yesterday’s noise might become tomorrow’s signal.

Whenever we employ simulations to investigate some real world phenomenon, a close correspondence between model and reality is necessary. Unacceptably large discrepancies between the two realms are known as a *simulation gap*, and the corresponding model is said to be *misspecified*. Model misspecification can arise from any of the three model components in isolation or simultaneously. A few illustrative examples show what can go wrong in practice:

- (i) **Misspecified Simulator.** In a model for the hydraulic conductivity of a medium, the spatial composition of the material is essential: A simulator relying on the assumption of homogeneity will wrongly predict the behavior of heterogeneous materials, biasing inference results in complex and arbitrary ways ([Schöniger et al., 2015](#); [Nowak and Guthke, 2016](#)).

- (ii) **Unexpected Contamination.** During an ongoing pandemic, data collection may be severely distorted, for example by noisy measurements, systematic underreporting, and delayed data transfer (Dehning et al., 2020), to name just a few. An epidemiological model disregarding these factors in $p(\xi | \theta)$ will produce erroneous inferences about key disease parameters, even if the underlying theory was otherwise a good approximation of the disease dynamics.
- (iii) **Misspecified Prior.** When the admissible region of the prior $p(\theta)$ is specified too large, – for example, allows negative mass – physically impossible simulations may arise.

Our generative model formulation is equivalent to the standard probabilistic factorization of the Bayesian joint distribution into likelihood and prior, $p(\theta, \mathbf{x} | \mathcal{M}) = p(\mathbf{x} | \theta, \mathcal{M}) p(\theta | \mathcal{M})$, where \mathcal{M} expresses the prior knowledge and assumptions embodied in the design of \mathcal{G} . This likelihood is obtained by marginalizing the joint distribution $p(\xi, \mathbf{x} | \theta, \mathcal{M})$ over all possible values of the nuisance parameters ξ , that is, over all possible execution paths of the simulation program, for fixed θ :

$$p(\mathbf{x} | \theta, \mathcal{M}) = \int_{\Xi} p(\xi, \mathbf{x} | \theta, \mathcal{M}) d\xi. \quad (2)$$

This integral is typically intractable (Cranmer et al., 2020), but we assume that it exists and is non-degenerate, that is, it defines a proper density over the constrained manifold $(g(\theta, \xi), \xi)$, and this density can be learned.

Whenever we model a real-world complex system, we assume an unknown (true) generator $\mathbf{x} = \mathbb{G}(\cdot)$, which yields an unknown (true) distribution $\mathbf{x} \sim p^\circ(\mathbf{x})$ and is available to the data analyst only via a finite realization (i. e., actually observed data). Then, using the Bayesian formulation, we say that a generative model \mathcal{G} is strictly well-specified if

$$p^\circ(\mathbf{x}) = p(\mathbf{x} | \mathcal{M}) \equiv \int_{\Theta} p(\mathbf{x} | \theta, \mathcal{M}) p(\theta | \mathcal{M}) d\theta \quad (3)$$

for every $\mathbf{x} \in \mathcal{X}$. Conversely, a generative model is misspecified if an observable $\mathbf{x} \in \mathcal{X}$ exists for which the above equality is violated. Since models necessarily simplify reality, the above criterion for well-specified models is often unattainable in practice. We therefore relax the requirement by quantifying a model’s degree of misspecification in terms of the information loss incurred by the simplification: For an acceptable upper bound ϑ on the information loss, a model is well-specified if $\mathbb{D}[p^\circ(\mathbf{x}) || p(\mathbf{x} | \mathcal{M})] < \vartheta$ and misspecified otherwise. The symbol \mathbb{D} denotes a divergence metric quantifying the “distance” between the data distribution implied by reality and the model-implied data distribution (the marginal likelihood). Notably, equality in Eq. 3 implies no information loss by modeling $p^\circ(\mathbf{x})$ with $p(\mathbf{x} | \mathcal{M})$ and thus a divergence of zero. A natural choice for \mathbb{D} would be a metric from the family of \mathcal{F} -divergences, such as the Kullback-Leibler (KL) divergence. However, since the practical computation of \mathcal{F} -divergences requires closed-form densities, and thus $p^\circ(\mathbf{x})$ to be analytically tractable, we prefer a probability integral metric, such as the Maximum Mean Discrepancy (MMD; Gretton et al., 2012). Using the kernel trick, the MMD can be expressed as

$$\text{MIMD}^2[p^\circ(\mathbf{x}) || p(\mathbf{x} | \mathcal{M})] = \mathbb{E}_{p^\circ(\mathbf{x})} [\kappa(\mathbf{x}, \mathbf{x}')] + \mathbb{E}_{p(\mathbf{x} | \mathcal{M})} [\kappa(\mathbf{x}, \mathbf{x}')] - 2\mathbb{E}_{\substack{\mathbf{x} \sim p^\circ(\mathbf{x}) \\ \mathbf{x}' \sim p(\mathbf{x} | \mathcal{M})}} [\kappa(\mathbf{x}, \mathbf{x}')] . \quad (4)$$

Crucially, this metric is practically tractable because it can be efficiently estimated via finite samples from $p^\circ(\mathbf{x})$ and $p(\mathbf{x} | \mathcal{M})$. In the above expression, $\kappa(\cdot, \cdot)$ is any positive definite kernel and the metric equals zero if and only if the two densities are equal (Gretton et al., 2012).

We use sums of Gaussian kernels with different widths σ_i as an established and flexible universal kernel (Muandet et al., 2017). However, Ardizzone et al. (2018) observe that kernels with heavier tails may improve performance by yielding more meaningful gradients for outliers. Thus, we repeated all experiments with a sum of inverse multiquadratic kernels (as proposed by Tolstikhin et al., 2017). The results are essentially equal to those obtained with sums of Gaussian kernels (cf. Appendix I).

3.2 Architectures for amortized inference

Our proposed method can be applied to any framework that uses learned summary statistics as an input to a neural posterior approximator. We will exemplarily outline the integration of our method into the BayesFlow (Radev et al., 2020a) and the SNPE-C (aka APT, Greenberg et al., 2019) methods.

BayesFlow The BayesFlow method consists of a summary network h_ψ and an inference network f_ϕ which jointly amortize a generative model \mathcal{G} . The summary network h_ψ transforms input data \mathbf{x} of variable size to a fixed-length representation $h_\psi(\mathbf{x})$. The inference network samples from an approximate posterior q_ϕ via a conditional invertible neural network (cINN, ?). Together, the two networks minimize the expected KL divergence between approximate and true simulation posterior, which reduces to

$$\psi^*, \phi^* = \min_{\psi, \phi} \mathbb{E}_{p(\boldsymbol{\theta}, \mathbf{x} | \mathcal{M})} \left[-\log q_\phi(\boldsymbol{\theta} | h_\psi(\mathbf{x}), \mathcal{M}) \right], \quad (5)$$

since the true posterior $p(\boldsymbol{\theta} | \mathbf{x}, \mathcal{M})$ does not depend on the trainable neural network parameters. We approximate this expectation via simulations from the generative model \mathcal{G} and repeat the process until convergence. This objective is self-consistent and results in correct amortized inference under optimal convergence (Radev et al., 2020a). However, simulation-based training takes the expectation with respect to the model $p(\boldsymbol{\theta}, \mathbf{x} | \mathcal{M})$, not the true distribution $p^\circ(\mathbf{x})$. Thus, optimal convergence does not imply correct posterior inference or faithful prediction in the real world when there is a simulation gap, that is, when the model \mathcal{G} deviates critically from the unknown true generator.

SNPE-C The SNPE-C method (Greenberg et al., 2019) iteratively transforms a proposal (prior) distribution $\hat{p}(\boldsymbol{\theta} | \mathcal{M})$ into the posterior $p(\boldsymbol{\theta} | \mathbf{x}_{obs}, \mathcal{M})$ induced by given data set \mathbf{x}_{obs} through a series of simulation-based training rounds. Typically, the approximate posterior after a given round is used as the proposal prior for the next round, resulting in a *semi-amortized* optimization criterion:

$$\psi^*, \phi^* = \min_{\psi, \phi} \mathbb{E}_{p(\mathbf{x} | \boldsymbol{\theta}, \mathcal{M}) \hat{p}(\boldsymbol{\theta} | \mathcal{M})} \left[-\log \hat{q}_\phi(\boldsymbol{\theta} | \mathbf{x}, \mathcal{M}) \right], \quad (6)$$

where $\hat{p}(\boldsymbol{\theta} | \mathcal{M})$ is the current proposal distribution and the approximate posterior $\hat{q}_\phi(\boldsymbol{\theta} | \mathbf{x}, \mathcal{M})$ is represented as a categorical distribution over a discrete set of *atomic proposals* in order to be tractable (Greenberg et al., 2019). If we set $\hat{p}(\boldsymbol{\theta} | \mathcal{M}) = p(\boldsymbol{\theta} | \mathcal{M})$ for all rounds and introduce a jointly trained summary network $h_\psi(\mathbf{x})$, then the optimization criterion in Eq. 6 is identical to that of BayesFlow (Eq. 5) and SNPE-C can perform fully amortized inference. Either way, the first round of SNPE-C always depends only on the simulator outputs, so simulation gaps can be equally problematic.

3.3 Structured summary statistics

The summary network h_ψ acts as an interface between the data \mathbf{x} and the inference network f_ϕ . Its role is to learn maximally informative summary vectors of fixed size S from complex and structured observations (e. g., sets of *i.i.d.* measurements or multivariate time series). Therefore, the summary network’s representation $h_\psi(\mathbf{x})$ is an adequate target to detect simulation gaps.

Specifically, we propose to prescribe an S -dimensional multivariate unit Gaussian distribution to the summary space, $p(h_\psi(\mathbf{x}) | \mathcal{M}) \approx \mathcal{N}(z_\mathbf{x} | \mathbf{0}, \mathbb{I})$, by minimizing the MMD between summary network outputs and random draws from a unit Gaussian distribution. To ensure that the learned summary vectors comply with the support of the Gaussian density, we introduce a linear (bottleneck) output layer with S units to the summary network. Thus, a random vector in summary space takes the form $h_\psi(\mathbf{x}) := (s_1, \dots, s_S) \in \mathbb{R}^S$. The extended optimization objective then becomes

$$\psi^*, \phi^* = \operatorname{argmin}_{\psi, \phi} \mathbb{E}_{p(\boldsymbol{\theta}, \mathbf{x} | \mathcal{M})} \left[-\log q_\phi(\boldsymbol{\theta} | h_\psi(\mathbf{x}), \mathcal{M}) \right] + \gamma \cdot \text{MMD}^2[p(h_\psi(\mathbf{x}) | \mathcal{M}) || p(\mathbf{z}_\mathbf{x})], \quad (7)$$

with a hyperparameter γ to control the relative weight of the MMD term. For other frameworks, the MMD term is added to the optimization objective analogously. Intuitively, this objective encourages the approximate posterior $q_\phi(\boldsymbol{\theta} | h_\psi(\mathbf{x}), \mathcal{M})$ to match the true posterior and the summary distribution $p(h_\psi(\mathbf{x}) | \mathcal{M})$ to match a unit Gaussian. Appendix A discusses the theoretical implications.

3.4 Detecting model misspecification

Once the simulation-based training phase is completed, we can generate a validation sample $\{\boldsymbol{\theta}^{(m)}, \mathbf{x}^{(m)}\}_{m=1}^M$ from our generative model \mathcal{G} and pass it through the summary network to obtain a sample of latent summary vectors $\{\tilde{\mathbf{z}}_\mathbf{x}^{(m)}\}_{m=1}^M$, where $\tilde{\mathbf{z}}_\mathbf{x} = h_\psi(\mathbf{x})$ denotes the output of the summary network. The properties of this sample contain important convergence information, which is a prerequisite for meaningful model comparison later on: If $\tilde{\mathbf{z}}_\mathbf{x}$ is approximately unit Gaussian, we can

assume a structured summary space given G . This enables model misspecification diagnostics via distribution checking during inference on real data.

Let $\{\mathbf{x}_{obs}^{(n)}\}_{n=1}^N$ be an observed sample, either simulated from a different generative model, or arising from real-world observations with an unknown generator. Before invoking the inference network, we pass this sample through the summary network to obtain $\{\tilde{\mathbf{z}}_{x_{obs}}^{(n)}\}_{n=1}^N$. We then compare the validation summary distribution $\{\tilde{\mathbf{z}}_x^{(m)}\}_{m=1}^M$ with the summary representation at inference time $\{\tilde{\mathbf{z}}_{x_{obs}}^{(n)}\}_{n=1}^N$ according to the sample-based MMD estimate $\widehat{\text{MMD}}(\tilde{\mathbf{z}}_x, \tilde{\mathbf{z}}_{x_{obs}})$ (cf. [Gretton et al., 2012](#)). Importantly, we are not limited to pre-determined sizes of simulated or real-world datasets, as the MMD estimator is defined for arbitrary M and N .¹

Whenever we estimate the MMD from finite data, its estimates vary according to a sampling distribution and we can resort to a sampling-based (frequentist) hypothesis test to determine the probability of observed MMD values under well-specified models. We can estimate the MMD sampling distribution under the null hypothesis (i. e., no simulation gap) from multiple sets of simulations from the generative model, $\{\tilde{\mathbf{z}}_x^{(m)}\}_{m=1}^M$ and $\{\tilde{\mathbf{z}}_x^{(n)}\}_{n=1}^N$, with M large and N equal to the number of real data sets. Based on the estimated sampling distribution, we can obtain a critical MMD value for a fixed Type I error probability (α) and compare it to the one estimated with the observed data. In general, a larger α -level corresponds to a more conservative modeling approach: A higher type I error probability implies that more tests reject the null hypothesis, which corresponds to more frequent model misspecification alarms and a higher chance that incorrect models will be recognised. Note, that the Type II error probability (β) of this test will generally be high (i. e., the *power* of the test will be low) whenever the number of real data sets N is very small. However, we show in **Experiment 2** that even as few as 5 real data sets suffice to achieve $\beta \approx 0$ for a complex model.

3.5 Posterior inference errors due to misspecified models

Given a generative model \mathcal{M} , the *correct posterior under the potentially misspecified model* $p(\boldsymbol{\theta} | \mathbf{x}, \mathcal{M})$ always exists even if \mathcal{M} is misspecified for the data \mathbf{x} . Obtaining a trustworthy approximation of the correct posterior is the fundamental basis for any follow-up inference (e. g., parameter estimation or model comparison) and must be at least an intermediate goal in real world applications. Assuming optimal convergence under a misspecified model \mathcal{M} , the amortized posterior $q_\phi(\boldsymbol{\theta} | \mathbf{z}_x = h_\psi(\mathbf{x}), \mathcal{M})$ still corresponds to the correct posterior $p(\boldsymbol{\theta} | \mathbf{x}, \mathcal{M})$, as any transformed \mathbf{x} arising from $p^\circ(\mathbf{x})$ has non-zero density in the latent Gaussian summary space.² Thus, the inference network should still be able to obtain the correct pushforward density under \mathcal{M} for any query \mathbf{x} . However, optimal convergence can never be achieved after finite training time, so we need to address its implications for the validity of amortized simulation-based posterior inference in practice.

Given finite training data, the summary and inference networks will mostly see simulations from the *typical set* $\mathcal{T}(\mathcal{G}) \subset \mathcal{X}$ of the generative model \mathcal{G} , that is, training instances whose self-information $-\log p(\mathbf{x} | \mathcal{M})$ is close to the entropy $\mathbb{E}[-\log p(\mathbf{x} | \mathcal{M})]$. In high dimensional problems, the typical set will comprise a rather small subset of the possible outcome space, determined by a complex interaction between the components of \mathcal{G} ([Betancourt, 2017](#)). Accordingly, good convergence in practice may mean that i) only observations from $\mathcal{T}(\mathcal{G})$ actually follow the approximate Gaussian in latent summary space and ii) the inference network has only seen enough training examples in $\mathcal{T}(\mathcal{G})$ to learn accurate posteriors for observables $\mathbf{x} \in \mathcal{T}(\mathcal{G})$.

In contrast, atypical or improbable outcomes occur rarely during simulation-based training and have negligible effect on the loss in Eq. 7. Consequently, posterior approximation errors for observations outside of $\mathcal{T}(\mathcal{G})$ can be large, simply because the networks have not yet converged in these unusual regions, and the highly non-linear mapping of the inference network still deviates considerably from the true solution. Better training methods might resolve this problem in the future, but for now our proposed MMD criterion reliably signals low fidelity posterior estimates by quantifying the “distance from the typical generative set” $\mathcal{T}(\mathcal{G})$ in the structured summary space.

Moreover, we hypothesize and demonstrate empirically in the following experiments that the difference between the true $p(\boldsymbol{\theta} | \mathbf{x}, \mathcal{M})$ and the approximate posterior $q_\phi(\boldsymbol{\theta} | h_\psi(\mathbf{x}), \mathcal{M})$ for misspecified

¹To allow MMD estimation for data sets with single instances ($N = 1$ or $M = 1$), we do not use the unbiased MMD version from [Gretton et al. \(2012\)](#). Singleton data sets are an important use case for our method in practice, and potential advantages of unbiased estimators do not justify exclusion of such data.

²We assume that we have no hard limits in the prior or simulator in \mathcal{G} .

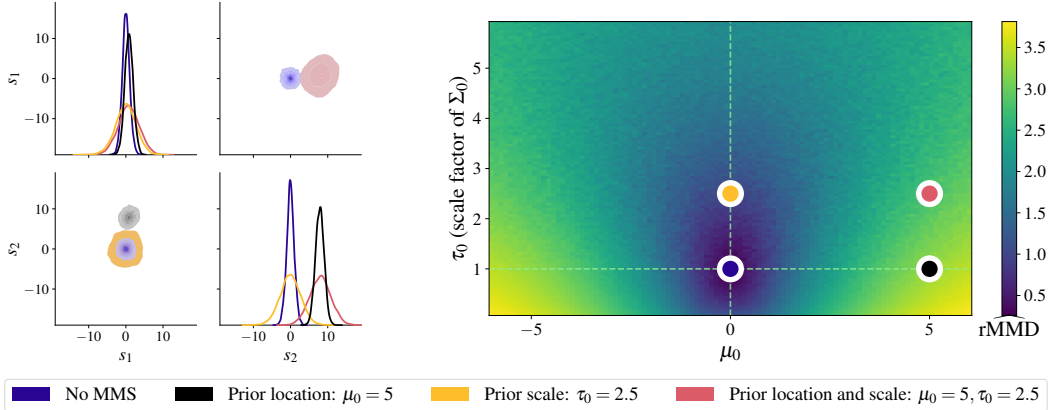


Figure 2: Prior misspecification can be detected with a minimal sufficient summary network ($S = 2$). **Left:** Pairplot of 10 000 summary space samples. All prior misspecifications are distinguishable from the typical latent generative space (blue). **Right:** MMD as a function of μ_0 (prior location) and τ_0 (scale factor in the mean prior). The MMD estimate increases as the simulation gap gets more severe. The colored dots correspond to the respective misspecified model configuration in the pairplot.

Table 1: Investigated model misspecifications in **Experiment 1**. The noise model \mathcal{M}_N is a mixture of a Gaussian and a Beta distribution, rescaled to $\pm 3\sigma_x$ to make detection harder.

Model (MMS)	Prior	Likelihood
\mathcal{M}^* (No MMS)	$\mu \sim \mathcal{N}(\mu_0 = \mathbf{0}, \Sigma_0 = \mathbb{I})$	$\mathbf{x}_k \sim \mathcal{N}(\mu, \Sigma = \mathbb{I})$
\mathcal{M}_P (Prior)	$\mu \sim \mathcal{N}(\mu_0 \neq \mathbf{0}, \Sigma_0 = \tau_0 \mathbb{I}), \tau_0 \in \mathbb{R}^+$	$\mathbf{x}_k \sim \mathcal{N}(\mu, \Sigma = \mathbb{I})$
\mathcal{M}_S (Simulator)	$\mu \sim \mathcal{N}(\mu_0 = \mathbf{0}, \Sigma_0 = \mathbb{I})$	$\mathbf{x}_k \sim \mathcal{N}(\mu, \Sigma = \tau \mathbb{I}), \tau \in \mathbb{R}^+$
\mathcal{M}_N (Noise)	$\mu \sim \mathcal{N}(\mu_0 = \mathbf{0}, \Sigma_0 = \mathbb{I})$	$\mathbf{x}_k \sim \lambda \cdot \text{Beta}(2, 5) + (1 - \lambda) \cdot \mathcal{N}(\mu, \Sigma = \mathbb{I})$

models increases as a function of MMD and thus also measures the amount of misspecification. Therefore, our MMD criterion serves a dual purpose in practice: It can uncover potential simulation gaps and, simultaneously, signal errors in posterior estimation.

4 Experiments

4.1 Experiment 1: multivariate normal distribution

Setup. We set the stage by estimating the posterior mean of a D -dimensional conjugate toy multivariate normal (MVN) model with a known analytic posterior in order to illustrate our method. The generative model is defined as

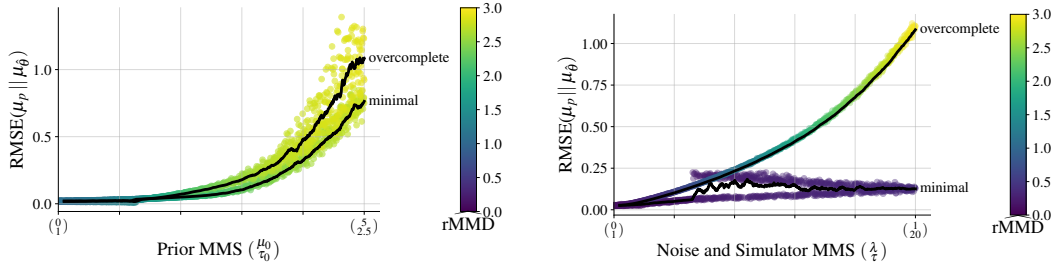
$$\mathbf{x}_k \sim \mathcal{N}(\mathbf{x} | \mu, \Sigma) \quad \text{for } k = 1, \dots, K \quad \text{with } \mu \sim \mathcal{N}(\mu | \mu_0, \Sigma_0) \quad (8)$$

For ease of visualization, we set $D = 2$ and simulate data sets of $K = 100$ observations each. We use a permutation invariant summary network (Bloem-Reddy and Teh, 2020) with $S = 2$ output dimensions, which equal the number of minimal sufficient statistics³ implied by the analytic posterior. We set the prior to a unit Gaussian and the likelihood covariance Σ to an identity matrix. The model \mathcal{M}^* used for training the networks as well as the types of misspecifications are outlined in Table 1. We conduct the experiment with BayesFlow as well as SNPE-C, both equipped with our adjusted optimization objective.⁴

Results. The BayesFlow network trained to minimize the augmented objective (Eq. 7) exhibits excellent recovery of the analytic posterior means when no misspecification is present (30min training

³Note that the terms “minimal”, “sufficient”, and “overcomplete” refer to the inference task and *not* to the data. Thus, $S = 2$ summary statistics are *sufficient* to solve the inference task, namely recover two means.

⁴BayesFlow is available at <https://github.com/stefanradev93/BayesFlow> (MIT license), SNPE-C is available in the sbi package at <https://github.com/mackelab/sbi> (AGPL-3.0 license).



(a) Prior misspecification: Both summary networks (minimal and overcomplete) detect increasingly severe misspecification through an elevated rMMD and lead to a higher posterior error (RMSE) of the inference network.

(b) Noise and simulator misspecification: While the minimal network exhibits poor detection, its posterior recovery is not impaired either. The overcomplete network captures increasingly severe misspecification but suffers from an increased posterior error (RMSE).

Figure 3: Posterior error (RMSE between analytic posterior means μ_p and approximate posterior means $\mu_{\hat{\theta}}$) as a function of model misspecification severity, as indexed by the MMD criterion.

time on a CPU). All prior misspecifications manifest in anomalies in the summary space which are directly detectable through visual inspection of the 2-dimensional summary space in Figure 2. Note, that the combined prior misspecification (location and scale) exhibits a summary space pattern that mirrors the location and scale of the respective location and scale misspecification. However, based on the 2-dimensional summary space, misspecifications in the fixed parameters of the likelihood (τ) and mixture noise are neither detectable through visual inspection, nor through increased MMD.

We then investigate the effect of an overcomplete summary space with respect to the inference task, namely $S = 4$ summary outputs with an otherwise equal architecture. The overcomplete summary space captures misspecifications in the noise and simulator through the MMD criterion (see Figure B.1b). Furthermore, the induced misspecifications in the noise distribution and simulator are visually detectable in the summary space samples (see Figure B.2). The 2-dimensional summary space fails to capture these misspecifications (see Figure B.1a).

Finally, we compute the error in posterior recovery via RMSE and MMD as a function of misspecification severity for both BayesFlow networks relying on a minimal ($S = 2$) or an overcomplete ($S = 4$) summary network. Figure 3 illustrates that a larger MMD estimate coincides with a larger error in posterior estimation across all model misspecifications for both summary networks. However, the minimal and overcomplete networks exhibit a drastically different behavior when processing data with misspecified noise and simulator (see Figure 3b). While the minimal summary network cannot detect noise or simulator simulation gaps, its posterior estimation performance is not heavily impaired either (see Figure 3b). On the other hand, the overcomplete summary network is able to capture noise and simulator misspecifications, but also incurs larger posterior inference error.

SNPE-C (APT). Our method successfully detects model misspecification in SNPE-C (Greenberg et al., 2019) with the proposed MMD criterion and a structured summary space (see Appendix C). The results are largely equivalent to those obtained with BayesFlow. The subtle differences are not soundly interpretable due to the architectural differences of the two frameworks.

Higher dimensions. We extended the toy model to higher dimensions and a more difficult task (i. e., recover information beyond first moments) in BayesFlow. Appendix D shows that our method successfully detects simulation gaps for a 5D Gaussian with a fully estimated covariance matrix.

4.2 Experiment 2: COVID-19 modeling

Setup. Compartmental models in epidemiology (CMs) are very popular for inferring relevant disease parameters, simulating possible outbreak scenarios, and projecting future outcomes (Dehning et al., 2020). Given the abundance of such models and their increasing complexity, the importance of detecting simulation gaps for trustworthy inference is two-fold. First, since substantial conclusions are based on the posterior distributions of model parameters, it is important that these distributions are formally correct even when models do not capture all relevant real-world factors. Second, given the

Table 2: Results for different variations of the COVID-19 compartmental model. We report the median and 95% CI of 100 bootstrap samples of $\widehat{\text{rMMD}}$ for each N (see Appendix F for details).

Model	Bootstrap $\widehat{\text{rMMD}}$			Power ($1 - \beta$)		
	$N = 1$	$N = 2$	$N = 5$	$N = 1$	$N = 2$	$N = 5$
\mathcal{M}^*	3.70 [3.65, 3.79]	2.61 [2.54, 2.91]	1.66 [1.59, 1.84]	—	—	—
\mathcal{M}_1	3.76 [3.72, 3.80]	2.86 [2.62, 3.16]	2.11 [1.82, 2.50]	.998	.958	≈ 1.0
\mathcal{M}_2	3.80 [3.73, 3.83]	2.81 [2.65, 3.00]	2.01 [1.82, 2.19]	.789	.804	≈ 1.0
\mathcal{M}_3	3.78 [3.74, 3.83]	2.81 [2.68, 3.11]	2.07 [1.92, 2.41]	.631	.690	≈ 1.0

dynamic aspect of these models, it is important to detect if an initially well-specified model becomes misspecified at a later time, so the model and its predictions can be amended.

As a final real-world example, we thus focus on a high-dimensional CM representing the early months of the COVID-19 pandemic in Germany (Radev et al., 2021b). Here, we investigate the utility of our distribution matching method to detect simulation gaps. To achieve this, we train a BayesFlow setup identical to Radev et al. (2021b) but using our new optimization objective (Eq. 7) to encourage a structured summary space (24h training time on NVIDIA GTX 1070Ti). We then simulate 1000 time-series from the original model \mathcal{M}^* and 1000 time-series from three misspecified models: i) a model \mathcal{M}_1 without an intervention sub-model; ii) a model \mathcal{M}_2 without an observation sub-model; iii) a model \mathcal{M}_3 without a latent “carrier” compartment (Dehning et al., 2020).

Results. Table 2 shows the MMD between the summary representation of $N = 1, 2, 5$ bootstrapped time series from each model and the summary representation of the 1000 time series from model \mathcal{M}^* . We also calculate the power ($1 - \beta$) of our hypothesis test for each misspecified model $\mathcal{M}_{j \in \{1, 2, 3\}}$ under the sampling distribution estimated from 1 000 samples of the 1 000 time series from \mathcal{M}^* at a type I error probability of $\alpha = .05$. We observe that the power of the test rapidly increases with more data sets and the Type II error probability (β) is essentially zero for as few as $N = 5$ time series (full power analysis results in Figure H.1).

As a next step, we pass the reported data between 1 March and 21 April 2020 (data from Dong et al., 2020, under CC BY 4.0 license) through the summary network and compute the critical MMD value for a sampling-based hypothesis test with an α -level of .05 (see Figure F.1). The observed MMD of the Germany data is below the critical MMD value, leading to the conclusion that the model is not misspecified for this time period. Finally, we perform linear dimensionality reduction (PCA) on the summary space and find that the first 40 principal components jointly explain 95% of the variance in the 192-dimensional summary space outputs. Thus, a 40-dimensional learned summary vector might provide a good approximation of the true (unknown) minimally sufficient summary statistics and render inference less fragile in the face of potential misspecifications.

5 Discussion

With this work, we approached a fundamental problem in amortized simulation-based Bayesian inference, namely, capturing posterior errors due to model misspecification. We proposed to increase the networks’ awareness of posterior errors by compressing simulations into a structured latent space induced by a modified optimization objective. We then applied the maximum mean discrepancy (MMD) estimator, equipped with a sampling-based hypothesis test, as a criterion to spotlight discrepancies between model-implied reality and actual observations in latent space. While we focused on the application to SNPE-C and BayesFlow, the proposed methods can be directly employed in other frameworks with learned neural summary statistics as well.

Our methods can be extended and modified in multiple ways. We optimized the latent data space towards a spherical Gaussian structure. However, our method should work with arbitrary latent data distributions. For example, heavy-tailed distributions (e. g., α -stable distributions with tunable tail parameters) might reduce the impact of outliers in latent space. Initial experiments indicate that such variations can lower posterior errors while still maintaining the ability to detect simulation gaps. The idea of Frazier et al. (2020) to detect simulation gaps by posterior discrepancies between differently configured approximator instances is interesting, and future endeavors might incorporate

this into simulation-based inference with neural networks. In addition, considerations on information geometry and non-Euclidean spaces might guide future research into building more flexible latent spaces and distance metrics ([Arvanitidis et al., 2021](#)).

Our methods are openly available (link redacted during review) and can be seamlessly integrated into an end-to-end workflow for amortized simulation-based inference.

References

- Alquier, P. and Ridgway, J. (2019). Concentration of tempered posteriors and of their variational approximations. *arXiv:1706.09293 [cs, math, stat]*. arXiv: 1706.09293.
- Ardizzone, L., Kruse, J., Wirkert, S. J., Rahner, D., Pellegrini, E. W., Klessen, R. S., Maier-Hein, L., Rother, C., and Köthe, U. (2018). Analyzing Inverse Problems with Invertible Neural Networks. *CoRR*, abs/1808.04730.
- Arvanitidis, G., González-Duque, M., Pouplin, A., Kalatzis, D., and Hauberg, S. (2021). Pulling back information geometry. *arXiv preprint arXiv:2106.05367*.
- Barnard, J., McCulloch, R., and Meng, X.-L. (2000). Modelling Covariance Matrices in Terms of Standard Deviations and Correlations, with Application To Shrinkage. *Statistica Sinica*, 10:1281–1311.
- Betancourt, M. (2017). A conceptual introduction to Hamiltonian Monte Carlo. *arXiv preprint*.
- Bieringer, S., Butter, A., Heimel, T., Höche, S., Köthe, U., Plehn, T., and Radev, S. T. (2021). Measuring QCD Splittings with Invertible Networks. *SciPost Physics Proceedings*, 10(6).
- Bloem-Reddy, B. and Teh, Y. W. (2020). Probabilistic Symmetries and Invariant Neural Networks. *J. Mach. Learn. Res.*, 21:90–1.
- Carpenter, B., Gelman, A., Hoffman, M. D., Lee, D., Goodrich, B., Betancourt, M., Brubaker, M., Guo, J., Li, P., and Riddell, A. (2017). Stan: A probabilistic programming language. *Journal of statistical software*, 76(1).
- Cranmer, K., Brehmer, J., and Louppe, G. (2020). The frontier of simulation-based inference. *Proceedings of the National Academy of Sciences*, 117(48):30055–30062.
- Dehning, J., Zierenberg, J., Spitzner, F. P., Wibral, M., Neto, J. P., Wilczek, M., and Priesemann, V. (2020). Inferring change points in the spread of COVID-19 reveals the effectiveness of interventions. *Science*, 369(6500).
- Dong, E., Du, H., and Gardner, L. (2020). An interactive web-based dashboard to track COVID-19 in real time. *The Lancet Infectious Diseases*, 20(5):533–534.
- Durkan, C., Murray, I., and Papamakarios, G. (2020). On contrastive learning for likelihood-free inference. In *International Conference on Machine Learning*, pages 2771–2781. PMLR.
- Frazier, D. T. and Drovandi, C. (2021). Robust Approximate Bayesian Inference With Synthetic Likelihood. *Journal of Computational and Graphical Statistics*, 30(4):958–976.
- Frazier, D. T., Robert, C. P., and Rousseau, J. (2020). Model misspecification in approximate Bayesian computation: consequences and diagnostics. *Journal of the Royal Statistical Society: Series B (Statistical Methodology)*, 82(2):421–444.
- Gonçalves, P. J., Lueckmann, J.-M., Deistler, M., Nonnenmacher, M., Öcal, K., Bassetto, G., Chintaluri, C., Podlaski, W. F., Haddad, S. A., Vogels, T. P., et al. (2020). Training deep neural density estimators to identify mechanistic models of neural dynamics. *Elife*, 9:e56261.
- Greenberg, D., Nonnenmacher, M., and Macke, J. (2019). Automatic posterior transformation for likelihood-free inference. In *International Conference on Machine Learning*, pages 2404–2414. PMLR.
- Gretton, A., Borgwardt, K., Rasch, M., Schölkopf, B., and Smola, A. (2012). A Kernel Two-Sample Test. *The Journal of Machine Learning Research*, 13:723–773.
- Grünwald, P., Van Ommen, T., et al. (2017). Inconsistency of Bayesian inference for misspecified linear models, and a proposal for repairing it. *Bayesian Analysis*, 12(4):1069–1103.
- Hermans, J., Begy, V., and Louppe, G. (2020). Likelihood-free mcmc with amortized approximate ratio estimators. In *International Conference on Machine Learning*, pages 4239–4248. PMLR.

- Lueckmann, J.-M., Goncalves, P. J., Bassetto, G., Öcal, K., Nonnenmacher, M., and Macke, J. H. (2017). Flexible statistical inference for mechanistic models of neural dynamics. *Advances in Neural Information Processing Systems*, 30.
- Mardia, K., Kent, J., and Bibby, J. (1979). *Multivariate analysis*. Probability and mathematical statistics. Acad. Press, London.
- Muandet, K., Fukumizu, K., Sriperumbudur, B., and Schölkopf, B. (2017). Kernel Mean Embedding of Distributions: A Review and Beyond. *Foundations and Trends® in Machine Learning*, 10(1-2):1–141.
- Murphy, K. (2007). Conjugate Bayesian analysis of the Gaussian distribution.
- Nowak, W. and Guthke, A. (2016). Entropy-based experimental design for optimal model discrimination in the geosciences. *Entropy*, 18(11):409–434.
- Papamakarios, G., Sterratt, D., and Murray, I. (2019). Sequential neural likelihood: Fast likelihood-free inference with autoregressive flows. In *The 22nd International Conference on Artificial Intelligence and Statistics*, pages 837–848. PMLR.
- Radev, S. T., D’Alessandro, M., Mertens, U. K., Voss, A., Köthe, U., and Bürkner, P.-C. (2021a). Amortized bayesian model comparison with evidential deep learning. *IEEE Transactions on Neural Networks and Learning Systems*.
- Radev, S. T., Graw, F., Chen, S., Mutters, N. T., Eichel, V. M., Bärnighausen, T., and Köthe, U. (2021b). OutbreakFlow: Model-based Bayesian inference of disease outbreak dynamics with invertible neural networks and its application to the COVID-19 pandemics in Germany. *PLOS Computational Biology*, 17(10):e1009472.
- Radev, S. T., Mertens, U. K., Voss, A., Ardizzone, L., and Köthe, U. (2020a). BayesFlow: Learning complex stochastic models with invertible neural networks. *IEEE Transactions on Neural Networks and Learning Systems*.
- Radev, S. T., Voss, A., Wieschen, E. M., and Buerkner, P.-C. (2020b). Amortized Bayesian Inference for Models of Cognition.
- Ratcliff, R. and McKoon, G. (2008). The Diffusion Decision Model: Theory and Data for Two-Choice Decision Tasks. *Neural Computation*, 20(4):873–922.
- Schöniger, A., Illman, W. A., Wöhling, T., and Nowak, W. (2015). Finding the right balance between groundwater model complexity and experimental effort via Bayesian model selection. *Journal of Hydrology*, 531:96–110.
- Shiono, T. (2021). Estimation of agent-based models using Bayesian deep learning approach of BayesFlow. *Journal of Economic Dynamics and Control*, 125:104082.
- Stan Development Team (2018). The Stan Core Library. Version 2.18.0.
- Stine, R. (1989). An Introduction to Bootstrap Methods. *Sociological Methods & Research*, 18(2-3):243–291.
- Thomas, O. and Corander, J. (2019). Diagnosing model misspecification and performing generalized Bayes’ updates via probabilistic classifiers. *arXiv preprint arXiv:1912.05810*.
- Tolstikhin, I., Bousquet, O., Gelly, S., and Schoelkopf, B. (2017). Wasserstein auto-encoders.
- Wiqvist, S., Frellsen, J., and Picchini, U. (2021). Sequential Neural Posterior and Likelihood Approximation. *arXiv preprint arXiv:2102.06522*.
- Zhang, F. and Gao, C. (2020). Convergence rates of variational posterior distributions. *The Annals of Statistics*, 48(4).

A Theoretical implications of the method

Attaining the global minimum of Eq. 7 with an arbitrarily expressive BayesFlow architecture $\{h_{\psi^*}, f_{\phi^*}, \mathcal{M}\}$ implies that i) the inference and summary network jointly amortize the correct posterior $p(\theta | \mathbf{x}, \mathcal{M})$ and ii) the summary network transforms $p(\mathbf{x} | \mathcal{M})$ into a unit Gaussian $p(\mathbf{z}_x = h_{\psi^*}(\mathbf{x})) = \mathcal{N}(\mathbf{z}_x | \mathbf{0}, \mathbb{I})$. According to (i), the set of inference network parameters ϕ^* is a minimizer of

$$\phi^* = \underset{\phi}{\operatorname{argmin}} \mathbb{E}_{p(\mathbf{z}_x)} \mathbb{E}_{p(\theta | \mathbf{z}_x)} \left[-\log q_{\phi}(\theta | \mathbf{z}_x) \right], \quad (9)$$

while (ii) ensures that $\operatorname{MMID}^2[p^{\circ}(h_{\psi^*}(\mathbf{x})) || p(\mathbf{z}_x)] > 0$ implies $\operatorname{MMID}^2[p^{\circ}(\mathbf{x}) || p(\mathbf{x} | \mathcal{M})] > 0$, since a deviation of $p^{\circ}(h_{\psi^*}(\mathbf{x}))$ from a unit Gaussian implies that the summary network is no longer transforming samples from $p(\mathbf{x} | \mathcal{M})$. Accordingly, $\operatorname{MMID}^2[p^{\circ}(h_{\psi^*}(\mathbf{x})) || p(\mathbf{z}_x)] > 0$ no longer guarantees that the inference network parameters ϕ^* are globally optimal. The preceding argumentation also motivates our augmented objective, since a divergence of $p^{\circ}(h_{\psi}(\mathbf{x}))$ from a unit Gaussian signals a deficiency in the assumed generative model \mathcal{G} and a need to revise the generative model. We also hypothesize and show empirically that we can successfully detect simulation gaps in practice even when convergence of the summary network outputs to a unit Gaussian is not strictly optimal (e. g., in the presence of correlations, cf. **Experiment 2** and [Appendix E](#)).

However, the converse will not hold true in general, in other words, $\operatorname{MMID}^2[p^{\circ}(\mathbf{x}) || p(\mathbf{x} | \mathcal{M})] > 0$ does *not* generally imply $\operatorname{MMID}^2[p^{\circ}(h_{\psi}(\mathbf{x})) || p(\mathbf{z}_x)] > 0$. To show this via a counter-example, consider the generative model \mathcal{G} defined by $x_1 \sim \mathcal{N}(\mu, \sigma^2 = 2)$, $x_2 \sim \mathcal{N}(\mu, \sigma^2 = 2)$, $\mu \sim \delta(0)$ for $N = 2$ observations and a single-output summary network, $S = 1$. Then, an optimal summary network outputs the minimal sufficient summary statistic $h_{\psi^*}(x_1, x_2) = \bar{x} \equiv (x_1 + x_2)/2$. Thus, $p(x_1, x_2 | \mathcal{M}) = \mathcal{N}(x_1 | 0, 2) \times \mathcal{N}(x_2 | 0, 2)$ and $p(\bar{x}) = \mathcal{N}(0, 1)$, since $\operatorname{Var}(\bar{x}) = \operatorname{Var}((x_1 + x_2)/2) = (\operatorname{Var}(x_1) + \operatorname{Var}(x_2))/2^2 = 1$, which implies $\operatorname{MMID}^2[p(h_{\psi^*}(x_1, x_2)) || \mathcal{N}(0, 1)] = 0$.

Now, suppose that the real data are actually generated by a different process given by $x_1 \sim \mathcal{N}(\mu, \sigma^2 = 1)$, and $x_2 \sim \mathcal{N}(\mu, \sigma^2 = 3)$, $\mu \sim \delta(0)$. Clearly, $p^{\circ}(x_1, x_2) = \mathcal{N}(x_1 | 0, 1) \times \mathcal{N}(x_2 | 0, 3) \neq p(x_1, x_2 | \mathcal{M})$ and so $\operatorname{MMID}^2[p^{\circ}(\mathbf{x}) || p(\mathbf{x} | \mathcal{M})] > 0$. However, using the same calculations as above, we find that $p^{\circ}(\bar{x}) = \mathcal{N}(0, 1)$ such that $\operatorname{MMID}^2[p^{\circ}(h_{\psi^*}(x_1, x_2)) || \mathcal{N}(0, 1)] = 0$, despite the fact that the assumed generative model is misspecified.

The above example also shows that learning *minimal sufficient summary statistics* might not be optimal for detecting simulation gaps. On the other hand, increasing the output dimensions of the summary network S would enable the network to learn structurally richer (overcomplete) sufficient summary statistics. The latter would be invariant to fewer misspecifications and thus more useful for uncovering simulation gaps. In the above example, an *overcomplete* summary network with $S = 2$ which simply copies and scales the two variables by their corresponding variances is able to detect the misspecification. Next, we describe how to detect simulation gaps during inference using finite realizations from \mathcal{G} and p° .

B Multivariate normal distribution: overcomplete summary statistics

Figure B.1 illustrates how prior misspecifications with respect to the simulator and noise are only detectable with overcomplete learned summary statistics. Figure B.2 shows the latent summary space when overcomplete summary statistics ($S = 4$) are used in **Experiment 1** to recover the means of a 2-dimensional normal distribution. Model misspecification with respect to both simulator and noise is detectable through anomalies in the latent summary space. Note that a network with $S = 2$ summary statistics and otherwise equivalent architecture could not capture these types of model misspecification.

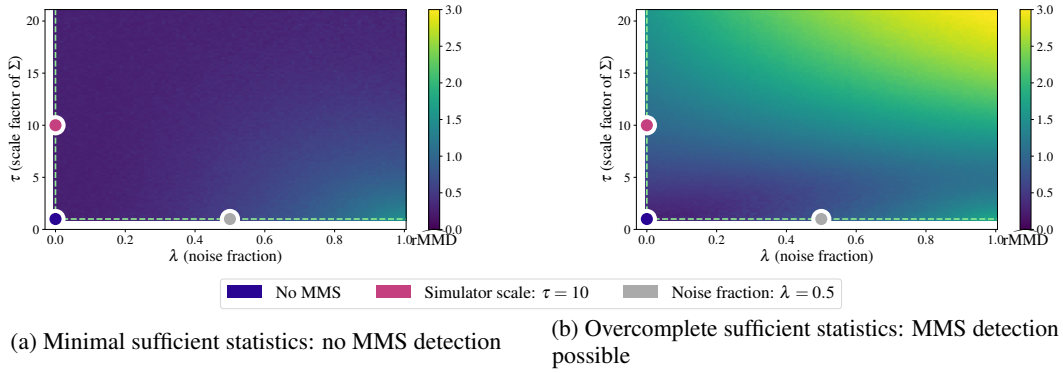


Figure B.1: $\widehat{\text{rMMD}}$ as a function of simulator and noise misspecification. While the minimal summary network yields essentially equal MMD estimates across the grid, the overcomplete summary network captures model misspecifications in both simulator and noise.

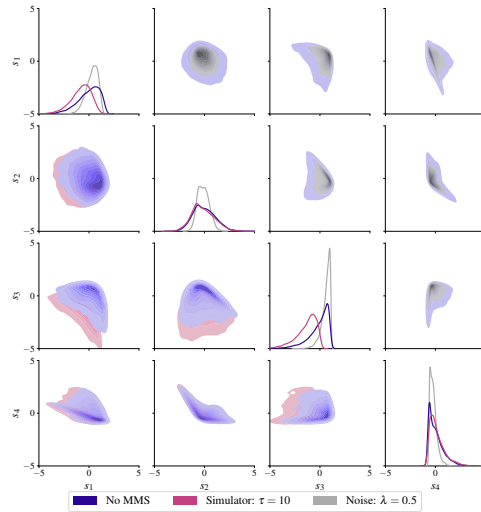


Figure B.2: Pairplot of 10 000 latent summary space samples from the overcomplete summary network. Both noise (orange) and simulator (pink) misspecifications are distinguishable from the typical latent generative space (blue).

C Replication of Experiment 1 with SNPE-C

In the following, we show the results of repeating **Experiment 1** with SNPE-C (APT; [Greenberg et al., 2019](#)) instead of BayesFlow for posterior inference. The results with respect to detection of simulation gaps are reliably equivalent to those obtained with the BayesFlow framework.

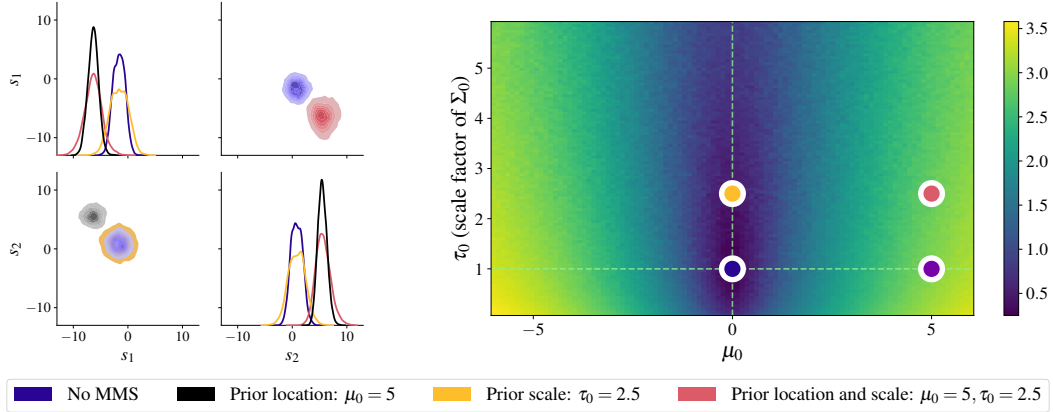
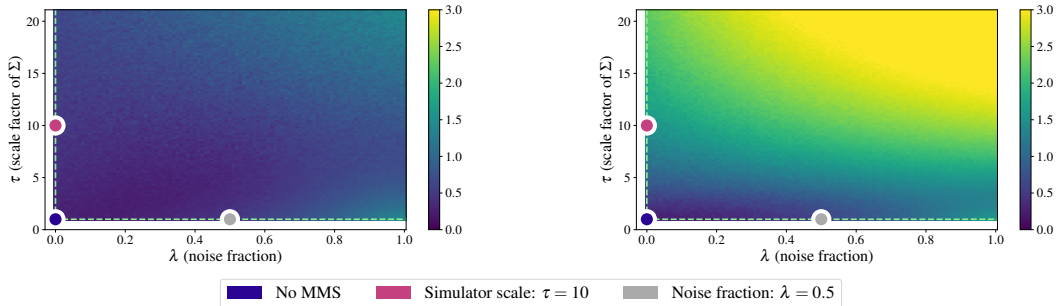


Figure C.1: In SNPE-C with learned summary statistics, prior misspecification can be reliably detected with a minimal sufficient network ($S = D = 2$) as well.

Left: Pairplot of 10 000 summary space samples. All prior misspecifications are distinguishable from the typical latent generative space (blue).

Right: $\widehat{\text{rMMD}}$ as a function of μ_0 (prior location) and τ_0 (scale factor in the mean prior). The MMD estimate increases as the simulation gap gets more severe. Colored dots correspond to the misspecified model configuration in the pairplot.



(a) Minimal sufficient statistics: no MMS detection

(b) Overcomplete sufficient statistics: MMS detection possible

Figure C.2: SNPE-C, $\widehat{\text{rMMD}}$ as a function of simulator and noise misspecification. While the minimal summary network yields essentially equal MMD estimates across the grid, the overcomplete summary network captures model misspecifications in both simulator and noise.

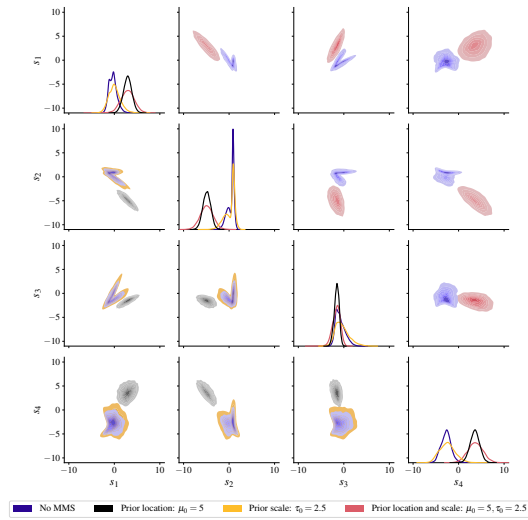


Figure C.3: SNPE-C, Pairplot of 10 000 latent summary space samples from the overcomplete summary network. Both noise (orange) and simulator (pink) misspecifications are distinguishable from the typical latent generative space (blue).

D Experiment: multivariate normal distribution, mean and full covariance recovery

As an extension to **Experiment 1**, we investigate the fully extended multivariate normal scenario where the mean and full covariance matrix need to be estimated. The mean vector and covariance matrix are drawn from a joint prior, namely a normal-inverse-Wishart distribution ($\text{N-}\mathcal{W}^{-1}$ (Barnard et al., 2000)). The normal-inverse-Wishart prior $\text{N-}\mathcal{W}^{-1}(\boldsymbol{\mu}, \boldsymbol{\Sigma} \mid \boldsymbol{\mu}_0, \lambda_0, \boldsymbol{\Psi}_0, \nu_0)$ implies a hierarchical prior. Suppose the covariance matrix

$$\boldsymbol{\Sigma} \sim \mathcal{W}^{-1}(\boldsymbol{\Sigma} \mid \boldsymbol{\Psi}_0, \nu_0) \quad (10)$$

has an inverse Wishart distribution and the mean vector

$$\boldsymbol{\mu} \sim \mathcal{N}(\boldsymbol{\mu} \mid \boldsymbol{\mu}_0, \frac{1}{\lambda_0} \boldsymbol{\Sigma}) \quad (11)$$

has a multivariate normal distribution, then the tuple $(\boldsymbol{\mu}, \boldsymbol{\Sigma})$ has a normal-inverse-Wishart distribution:

$$(\boldsymbol{\mu}, \boldsymbol{\Sigma}) \sim \text{N-}\mathcal{W}^{-1}(\boldsymbol{\mu}, \boldsymbol{\Sigma} \mid \boldsymbol{\mu}_0, \lambda_0, \boldsymbol{\Psi}_0, \nu_0) \quad (12)$$

Finally, the likelihood is Gaussian:

$$\mathbf{x}_k \sim \mathcal{N}(\boldsymbol{\mu}, \boldsymbol{\Sigma}) \quad \text{for } k = 1, \dots, K \quad (13)$$

We apply the BayesFlow method to recover the posterior mean and covariance of a multivariate normal distribution (MVN). For a D -variate Gaussian with random means and random covariance, BayesFlow needs to learn $1 + \dots + D$ covariances and D means. We set the number of summary statistics to $S = 40$, equal to twice the sufficient size for the 5-variate Gaussian. For a multivariate Gaussian with unknown mean and unknown covariance matrix, the analytic joint posterior $p(\boldsymbol{\mu}_p, \boldsymbol{\Sigma}_p \mid \{\mathbf{x}_k\}_{k=1}^K)$ has a closed form, following a normal-inverse Wishart distribution again:

$$\begin{aligned} (\boldsymbol{\mu}_p, \boldsymbol{\Sigma}_p \mid \{\mathbf{x}_k\}_{k=1}^K) &\sim \text{N-}\mathcal{W}^{-1}(\boldsymbol{\mu}_p, \boldsymbol{\Sigma}_p \mid \boldsymbol{\mu}_K, \lambda_K, \boldsymbol{\Psi}_K, \nu_K) \quad \text{with} \\ \boldsymbol{\mu}_K &= \frac{\lambda_0 \boldsymbol{\mu}_0 + K \bar{\mathbf{x}}}{\lambda_0 + K} \\ \lambda_K &= \lambda_0 + K \\ \nu_K &= \nu_0 + K \\ \boldsymbol{\Psi}_K &= \boldsymbol{\Psi}_0 + \sum_{k=1}^K (\mathbf{x}_k - \bar{\mathbf{x}})(\mathbf{x}_k - \bar{\mathbf{x}})^T + \frac{\lambda_0 K}{\lambda_0 + K} (\bar{\mathbf{x}} - \boldsymbol{\mu}_0)(\bar{\mathbf{x}} - \boldsymbol{\mu}_0)^T \end{aligned} \quad (14)$$

The marginal posteriors for $\boldsymbol{\mu}_p$ and $\boldsymbol{\Sigma}_p$ then follow as (Murphy, 2007):

$$\begin{aligned} \boldsymbol{\mu}_p &\sim t_{\nu_K - D - 1} \left(\boldsymbol{\mu}_p \mid \boldsymbol{\mu}_K, \frac{\boldsymbol{\Psi}_K^{-1}}{\lambda_K (\nu_K - D + 1)} \right) \\ \boldsymbol{\Sigma}_p &\sim \mathcal{W}^{-1}(\boldsymbol{\Sigma}_p \mid \boldsymbol{\Psi}_K, \nu_K) \end{aligned} \quad (15)$$

The model \mathcal{M}^* used for training the networks as well as the types of induced model misspecifications are outlined in Table 3.

Table 3: Investigated model misspecifications (MMS) for the 5-dimensional Gaussian with fully estimated covariance matrix. A sample from the noise model \mathcal{M}_N is simulated by randomly choosing a fraction $\lambda \in [0, 1]$ of the Gaussian data \mathbf{x} and replacing it with samples from $\boldsymbol{\eta} \sim \text{Beta}(2, 5)$ which is rescaled to $\pm 3\sigma_{\mathbf{x}}$ in order to match the data’s scale.

Model (MMS)	Prior	Likelihood
\mathcal{M}^* (No MMS)	$(\boldsymbol{\mu}, \boldsymbol{\Sigma}) \sim \text{N-}\mathcal{W}^{-1}(\boldsymbol{\mu}_0 = \mathbf{0}, \lambda_0 = 5, \boldsymbol{\Psi} = \mathbb{I}, \nu = 10)$	$\mathbf{x}_k \sim \mathcal{N}(\boldsymbol{\mu}, \boldsymbol{\Sigma})$
\mathcal{M}_P (Prior)	$(\boldsymbol{\mu}, \boldsymbol{\Sigma}) \sim \text{N-}\mathcal{W}^{-1}(\boldsymbol{\mu}_0 \neq \mathbf{0}, \lambda_0 = 5, \boldsymbol{\Psi} = \tau_0 \mathbb{I}, \nu = 10)$	$\mathbf{x}_k \sim \mathcal{N}(\boldsymbol{\mu}, \boldsymbol{\Sigma})$
\mathcal{M}_S (Simulator)	$(\boldsymbol{\mu}, \boldsymbol{\Sigma}) \sim \text{N-}\mathcal{W}^{-1}(\boldsymbol{\mu}_0 = \mathbf{0}, \lambda_0 = 5, \boldsymbol{\Psi} = \mathbb{I}, \nu = 10)$	$\mathbf{x}_k \sim t_{\text{df}}(\boldsymbol{\mu}, \boldsymbol{\Sigma}), \quad \text{df} \in \mathbb{N}_{>0}$
\mathcal{M}_N (Noise)	$(\boldsymbol{\mu}, \boldsymbol{\Sigma}) \sim \text{N-}\mathcal{W}^{-1}(\boldsymbol{\mu}_0 = \mathbf{0}, \lambda_0 = 5, \boldsymbol{\Psi} = \mathbb{I}, \nu = 10)$	$\mathbf{x}_k \sim \lambda \cdot \text{Beta}(2, 5) + (1 - \lambda) \cdot \mathcal{N}(\boldsymbol{\mu}, \boldsymbol{\Sigma})$

In the evaluation, we compare the means of BayesFlow’s predicted posterior samples with the first moment of the respective marginal analytic posterior from Equation 15. We evaluate correlation

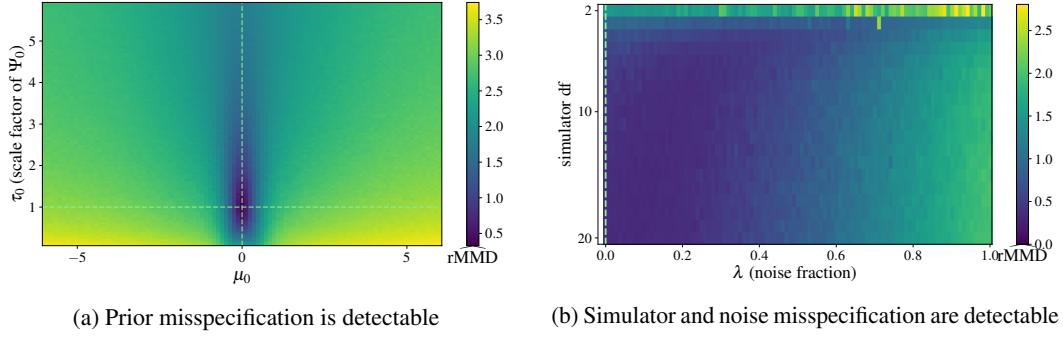


Figure D.1: $\widehat{\text{rMMD}}$ as a function of model misspecification with respect to the prior (left) as well as simulator and noise (right). All induced model misspecifications are detectable through the proposed detection criterion.

matrices with standard deviations on the diagonal. For the t distributed posterior mean and inverse-Wishart distributed posterior covariance, we obtain (Mardia et al., 1979):

$$\begin{aligned}\mathbb{E}(\boldsymbol{\mu}_p) &= \boldsymbol{\mu}_K \\ \mathbb{E}(\boldsymbol{\Sigma}_p) &= \frac{\boldsymbol{\Psi}_K}{\nu_K - D - 1}\end{aligned}\tag{16}$$

The converged BayesFlow network can recover the analytic posterior means as well as standard deviations and the correlation structure when no model misspecification is present. The performance decreases when model misspecification occurs. Since the summary space comprises $S = 40$ dimensions, visual inspection is no longer feasible. In the following, we inspect the effect of different degrees of model misspecification on the proposed $\widehat{\text{rMMD}}$ criterion (see Figure D.1). Both induced prior misspecifications are detectable through an increased $\widehat{\text{rMMD}}$. Model misspecifications through a heavy-tailed likelihood function (i. e., $\text{df} = 2$ in the context of a Student- t distribution) in the simulator are detectable as well. Increasing mixture weight λ of the Beta noise variate $\boldsymbol{\eta}$ leads to increased MMD values, rendering the investigated noise misspecifications detectable.

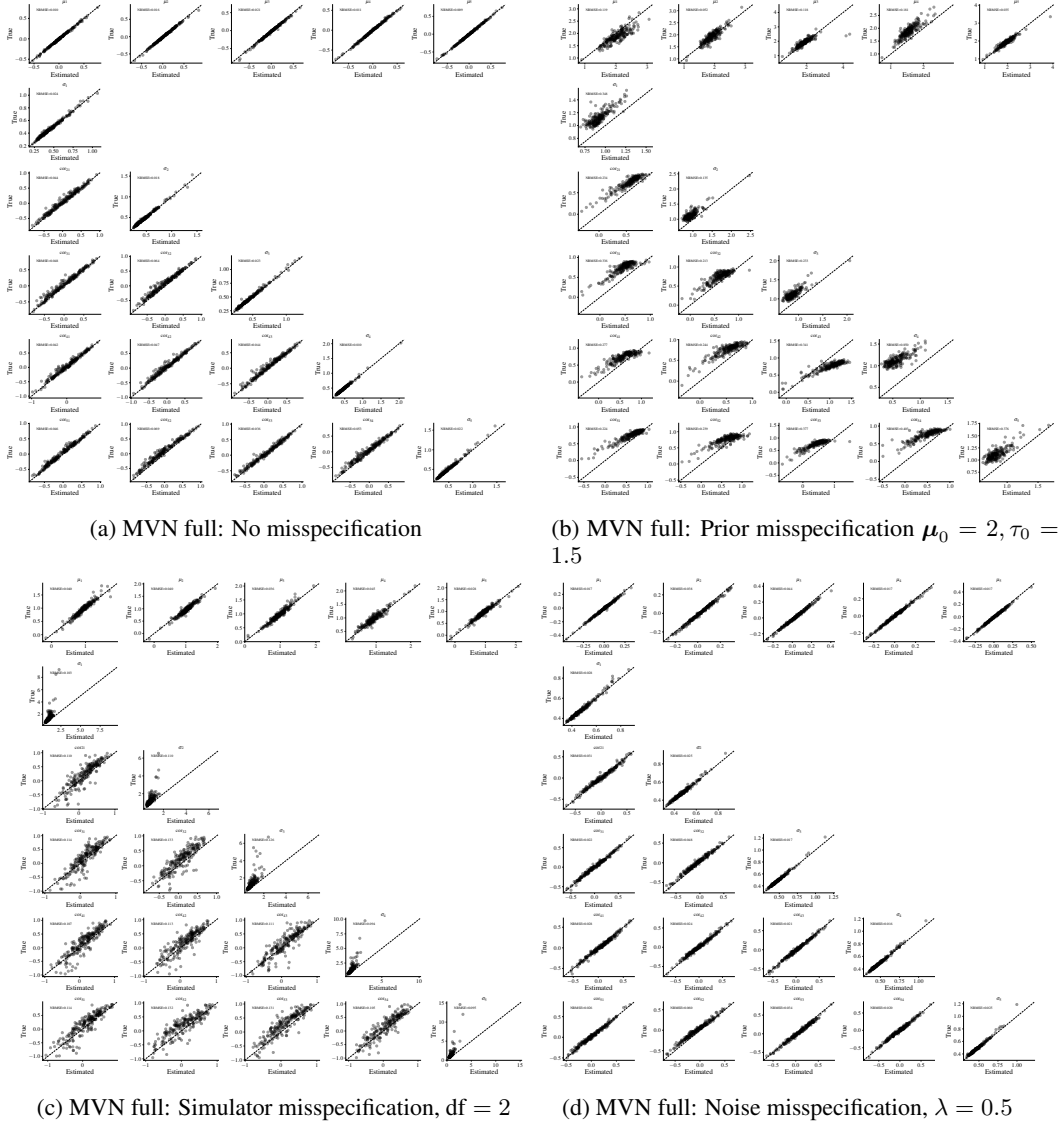


Figure D.2: MVN full covariance: Performance in recovering the means and covariance matrix under model misspecification

E Experiment: drift diffusion model

Aims. This experiment aims to i) apply the new optimization objective to a complex model of decision making; ii) illustrate the effect of dimensionality reduction (principal component analysis); iii) tackle strategies to determine the required number of learned summary statistics in more complex applications; iv) compare the posterior estimation of BayesFlow under a misspecified model with the estimation provided by the Stan implementation of HMC-MCMC (Carpenter et al., 2017; Stan Development Team, 2018) as a current gold-standard for Bayesian inference.

Setup. We focus on the drift diffusion model (DDM) – a cognitive model describing reaction times (RTs) in binary decision tasks (Ratcliff and McKoon, 2008) which is well amenable to amortized inference (Radev et al., 2020b). The DDM assumes that perceptual information for a choice alternative accumulates continuously according to a Wiener diffusion process. Thus, the change in information dx_j in experimental condition j follows a random walk with drift and Gaussian noise:

$$dx_j = vdt + \xi\sqrt{dt} \quad \text{with} \quad \xi \sim \mathcal{N}(0, 1) \quad (17)$$

Our model implementation assumes five free parameters $\theta = (v_1, v_2, a_1, a_2, t_0)$ which produce 2-dimensional data stemming from two simulated conditions. The starting point of the evidence accumulation process is unbiased, $x_{t=0} = \frac{a}{2}$. During training, the parameter priors are:

$$\begin{aligned} v_1, v_2 &\sim \Gamma(5, 0.5) \\ a_1, a_2 &\sim \Gamma(5, 0.5) \\ t_0 &\sim \Gamma(5, 0.5) \end{aligned} \quad (18)$$

The summary network is a permutation-invariant network which reduces *i. i. d.* RT data sets to 10–dimensional vectors. We realize a simulation gap by simulating typically observed contaminants: fast guesses (e. g., due to inattention), very slow responses (e. g., due to mind wandering), or a combination of the two. Accordingly, we first generate uncontaminated data \mathbf{x}^* from the well-specified generative model. Second, we randomly choose a fraction $\lambda \in [0, 1]$ of the data \mathbf{x}^* . Third, we replace this data fraction with contaminants ξ^o whose distribution depends on the quantiles of the uncontaminated data⁵:

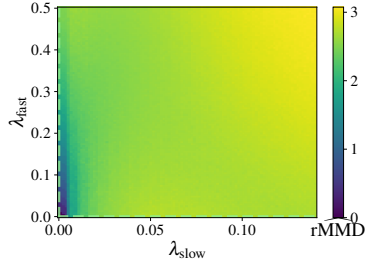
$$\begin{aligned} \text{Fast guesses:} \quad \xi^o &\sim \mathcal{U}(0.1, Q_{10}(\mathbf{x}^*)) \\ \text{Slow responses:} \quad \xi^o &\sim \mathcal{U}(Q_{75}(\mathbf{x}^*), 10) \end{aligned} \quad (19)$$

For the comparison with Stan, we simulate 100 uncontaminated DDM data sets and three scenarios (fast guesses, slow responses, fast and slow combined) with a fraction of $\lambda = 0.1$ contaminants.

Results. During inference, our criterion reliably detects the induced misspecifications: Increasing fractions λ of contaminants (fast, slow, and combined) manifest themselves in increasing MMD values (see Figure E.1a). The results of applying PCA to the summary network outputs $\{\tilde{\mathbf{z}}_{\mathbf{x}_{obs}}^{(n)}\}_{n=1}^N$ for the well-specified model (no contamination) are illustrated in Figure E.1b. We observe that the first five principal components exhibit a large overlap with the true model parameters θ and jointly account for 85% of the variance in the summary output. Furthermore, the drift rates and decision thresholds within conditions are entangled (i. e., v_1, a_1 and v_2, a_2). This entanglement mimics the strong posterior correlations observed between these two parameters. In practical applications, dimensionality reduction might act as a guideline for determining the number of minimally sufficient summary statistics or parameter redundancies for a given problem.

For the comparison with Stan, we juxtapose 4 000 samples from the neural network’s approximate posterior q_ϕ with 4 000 samples obtained from the Stan sampler after ensuring MCMC convergence and sufficient sampling efficiency for each data set in each simulated scenario (see Figure E.2 for an illustration). Because Stan is currently considered state-of-the-art for likelihood-based Bayesian

⁵ $Q_k(\mathbf{x}^*)$ denotes the k^{th} percentile of \mathbf{x}^* . The asymmetry in percentiles between fast and slow responses arises from the inherent positive skewness of reaction time distributions. The fixed upper limit of slow response contamination is motivated by the maximum number of iterations of the utilized diffusion model simulator. The contamination procedure is executed separately for each condition and response type. If an experiment features both fast and slow contamination, the fraction λ is equally split between fast and slow contamination. The uncontaminated data set is generated once and acts as a baseline for all analyses of an experiment, resulting in a baseline MMD of 0 since \mathbf{x}^* is unaltered if $\lambda = 0$.



(a) rMMD estimate by degree of contamination. Dashed lines represent the respective parameter value in the well-specified model without contamination, namely $\lambda_{\text{slow}} = \lambda_{\text{fast}} = 0$.

	PC1	PC2	PC3	PC4	PC5	PC6	PC7	PC8	PC9	PC10
ν_1	-0.03	-0.29	-0.48	-0.58	-0.23	-0.06	0.05	0.03	0.07	0.02
ν_2	-0.00	-0.71	-0.06	0.44	-0.14	-0.04	0.09	0.00	0.08	0.04
a_1	0.10	-0.05	0.68	-0.21	-0.48	0.15	0.15	-0.10	0.02	0.13
a_2	0.04	0.49	-0.39	0.33	-0.50	0.06	0.19	0.01	0.04	0.02
t_0	0.99	-0.01	-0.07	-0.00	0.06	-0.03	-0.02	0.02	-0.02	0.00
$\sum R^2$	0.31	0.47	0.60	0.73	0.85	0.95	0.99	1.00	1.00	1.00

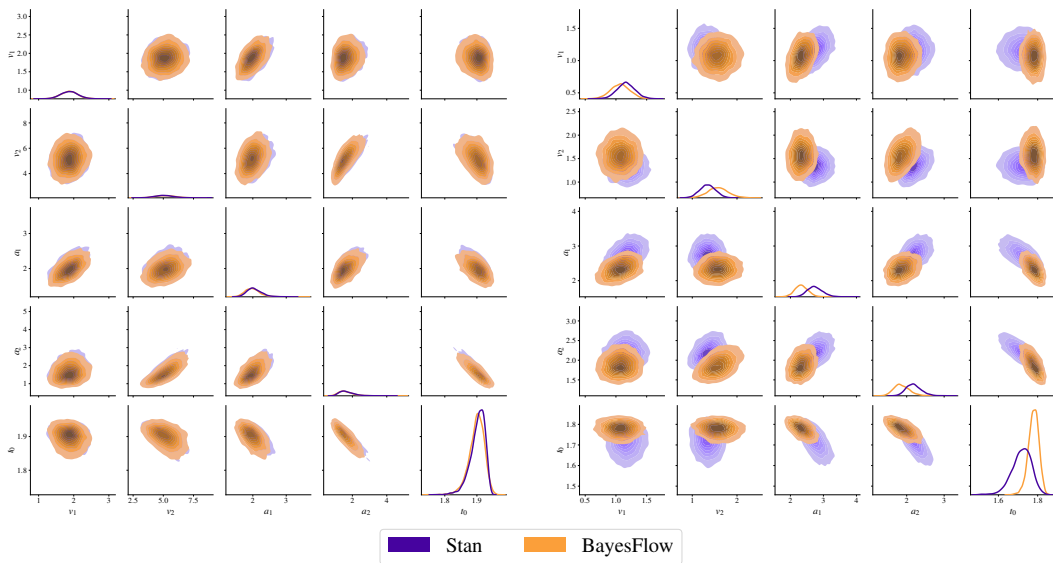
(b) Correlation between model parameters θ and principal components (PCs). The cumulative explained variance ratio w.r.t. the summary network outputs $\{\tilde{z}_{x_{obs}}^{(n)}\}_{n=1}^N$ is denoted as $\sum R^2$.

Figure E.1: Results of the Drift Diffusion Model experiment.

Table 4: Posterior error as the estimated rMMD (median and 95% confidence interval) between samples from BayesFlow’s approximate posterior q_ϕ and samples from the Stan sampler. The bootstrapped rMMD values (median and 95% confidence interval) for the summary space representation of the 100 investigated data sets and 1 000 samples from the uncontaminated model illustrate that posterior errors are mirrored by anomalies in the neural network’s summary space and thus detectable.

Model (Contamination)	Posterior error $\widehat{\text{rMMD}}$	Summary space $\widehat{\text{rMMD}}$
Uncontaminated	0.25 [0.13, 0.56]	0.45 [0.42, 0.52]
Fast contaminants	2.66 [1.44, 3.40]	2.68 [2.61, 2.74]
Slow contaminants	0.55 [0.23, 1.01]	1.18 [1.13, 1.26]
Fast and slow contaminants	1.90 [0.83, 3.18]	2.33 [2.19, 2.43]

inference, we assume the Stan samples are representative of the *true posterior* and compute the average rMMD estimate between the BayesFlow and Stan posterior estimates. Under no model misspecification, the posterior samples from BayesFlow and Stan match almost perfectly (see Figure E.2a). In contrast, the results in Figure E.2b and Table 4 clearly indicate that the amortized BayesFlow posteriors deteriorate as a result of the induced misspecification. Moreover, these results closely mirror the overall detectability of misspecification obtained by matching the summary representations of 1000 data sets from the uncontaminated process with the representations of the 100 data sets for each of the above scenarios via rMMD (see Table 4).



(a) No contamination, the approximate posteriors between Stan and BayesFlow are essentially equal, $\widehat{\text{rMMD}} = 0.034$

(b) Slow contamination ($\lambda = 10\%$), the approximate posteriors between Stan and BayesFlow differ by $\widehat{\text{rMMD}} = 0.854$

Figure E.2: Example comparison of the approximate posteriors from Stan and BayesFlow for an uncontaminated data set (left) as well as the contaminated version of the same data set (right; slow contamination).

F Details of Experiment 2 (COVID-19 time series)

Bootstrapping procedure

In **Experiment 2**, we estimate a sampling distribution of $\widehat{\text{rMMD}}$ between samples from \mathcal{M}^* and an observational model \mathcal{M}_{obs} . Since simulating time series from the compartmental models is time-consuming, we opt for bootstrapping (Stine, 1989) on 1 000 pre-simulated time series $\{\mathbf{x}^{*(i)}\}_{i=1}^{1000}$ from \mathcal{M}^* and 1 000 pre-simulated time series $\{\mathbf{x}_{\text{obs}}^{(j)}\}_{j=1}^{1000}$ from \mathcal{M}_{obs} . In each bootstrapping iteration, we draw 1 000 samples (with replacement) from $\{\mathbf{x}^{*(i)}\}_{i=1}^{1000}$ as well as $N \in \{1, 2, 5\}$ samples (with replacement) from $\{\mathbf{x}_{\text{obs}}^{(j)}\}_{j=1}^{1000}$ and calculate $\widehat{\text{rMMD}}$ between the sets of bootstrap samples.

Sampling distribution of MMD under the null hypothesis

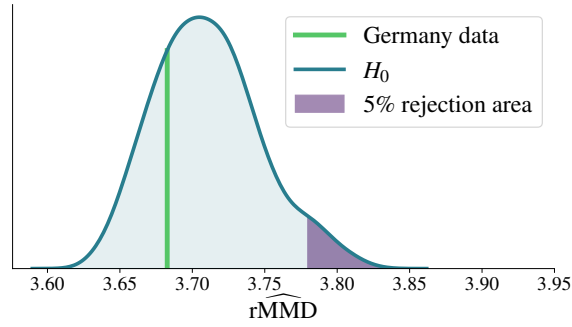
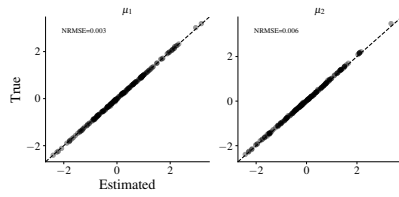
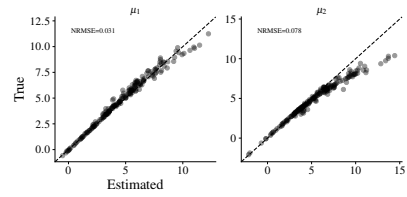


Figure F.1: Representation of Germany's COVID-19 time series with respect to the MMD distribution under the null hypothesis $H_0 : p^\circ(\mathbf{x}) = p(\mathbf{x} | \mathcal{M}^*)$.

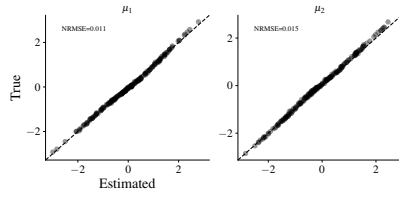
G Performance under model misspecification



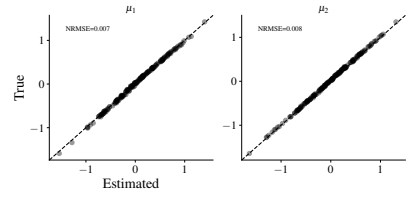
(a) MVN: no misspecification



(b) MVN: Prior misspecification $\mu_0 = 5, \tau_0 = 2.5$



(c) MVN: Simulator misspecification $\tau = 10.0$



(d) MVN: Noise misspecification, $\lambda = 0.5$

Figure G.1: Multivariate Normal Distributions: Performance in recovering the means (**Experiment 1**)

H COVID: detailed power analysis results

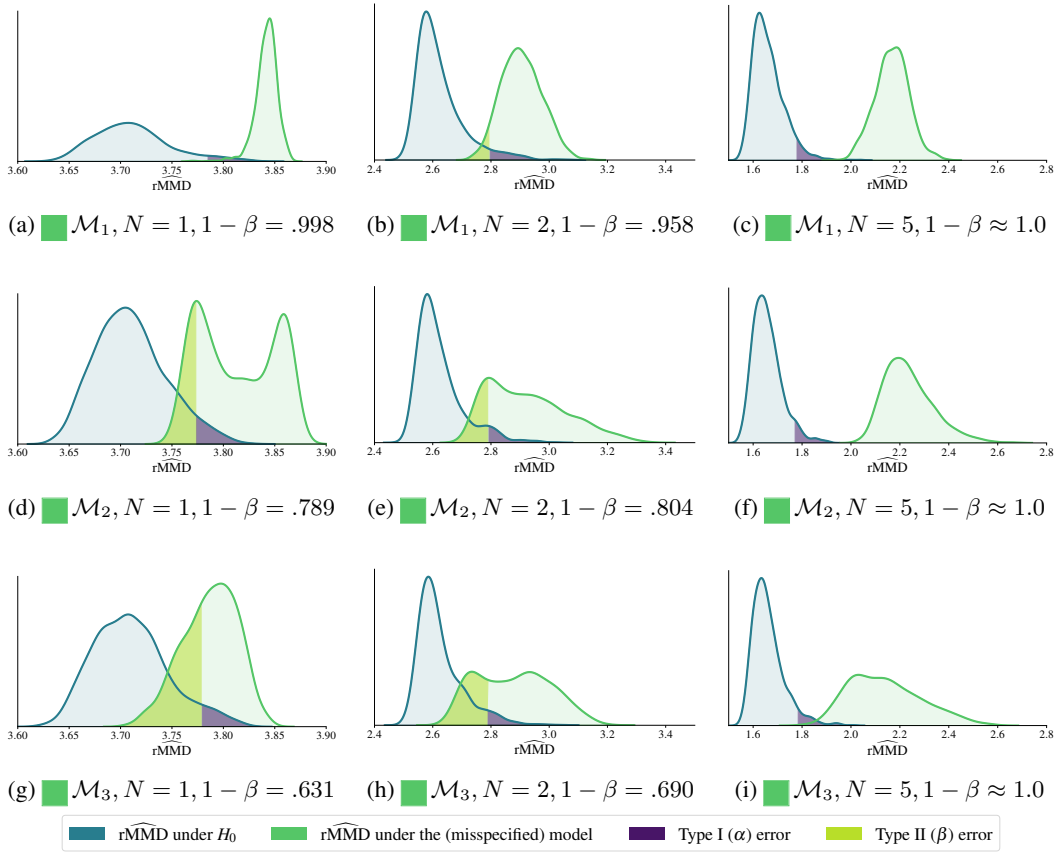


Figure H.1: Detailed illustration of the power analysis in **Experiment 2**.

I Inverse multiquadratic kernel

This appendix shows results of **Experiment 1** and **Experiment 2** when the sum of Gaussian kernels in the computation of the Maximum Mean Discrepancy (Equation 4) is replaced by a sum of inverse multiquadratic kernels.

I.1 Inverse multiquadratic kernel in Experiment 1

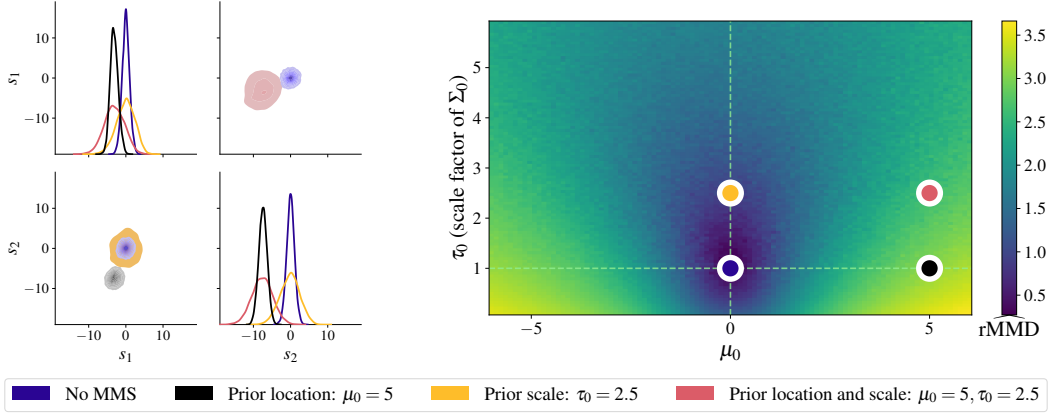
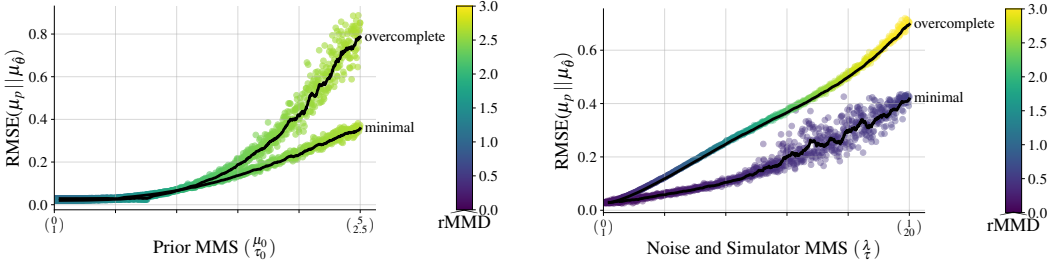


Figure I.1: Inverse multiquadratic kernel. Prior misspecification can be reliably detected with a minimal sufficient summary network ($S = D = 2$).

Left: Pairplot of 10 000 summary space samples. All prior misspecifications are distinguishable from the typical latent generative space (blue).

Right: $\widehat{\text{rMMD}}$ as a function of μ_0 (prior location) and τ_0 (scale factor in the mean prior). The $\widehat{\text{rMMD}}$ estimate increases as the simulation gap gets more severe. The colored dots correspond to the respective misspecified model configuration in the pairplot.



(a) Prior misspecification: Both summary networks (minimal and overcomplete) detect increasingly severe misspecification through an elevated rMMD and lead to a higher posterior error (RMSE) of the inference network.

(b) Noise and simulator misspecification: While the minimal network exhibits poor detection, its posterior recovery is not impaired either. The overcomplete network captures increasingly severe misspecification but suffers from an increased posterior error (RMSE).

Figure I.2: Inverse multiquadratic kernel. Posterior error (difference between analytic posterior means μ_p and the approximate posterior means μ_θ) as a function of model misspecification severity, as indexed by the $\widehat{\text{rMMD}}$ criterion.

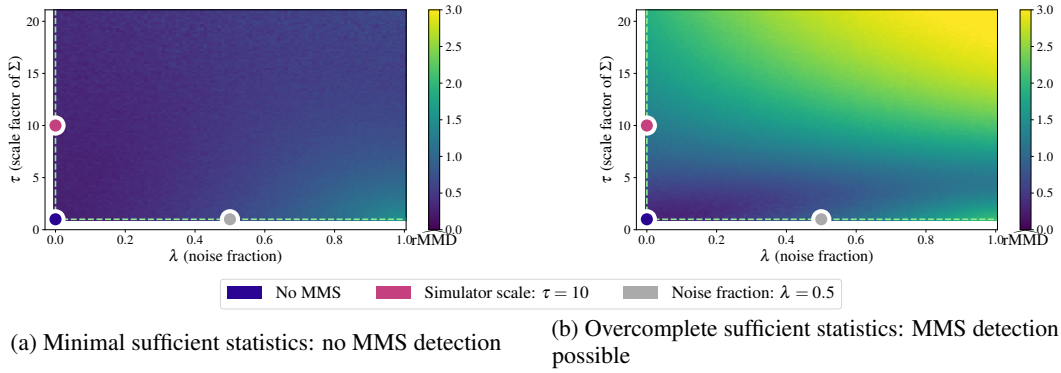


Figure I.3: Inverse multiquadric kernel, \widehat{rMMD} as a function of simulator and noise misspecification. While the minimal summary network yields essentially equal MMD estimates across the grid, the overcomplete summary network captures model misspecifications in both simulator and noise.

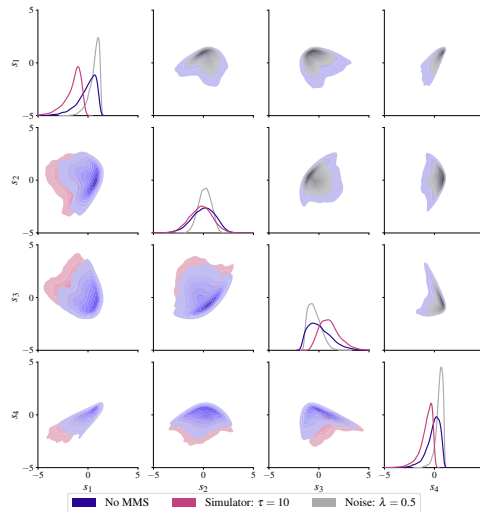


Figure I.4: Inverse multiquadric kernel. Pairplot of 10 000 latent summary space samples from the overcomplete summary network. Both noise (orange) and simulator (pink) misspecifications are distinguishable from the typical latent generative space (blue).

I.2 Inverse multiquadratic kernel in Experiment 2

Table 5: Results for different variations of the COVID-19 compartmental model with an inverse multiquadratic kernel. We report the median and 95% CI of 100 bootstrap samples of $\widehat{\text{rMMD}}$ for each N (see Appendix F for a detailed description of the procedure).

Model	Bootstrap $\widehat{\text{rMMD}}$			Power ($1 - \beta$)		
	$N = 1$	$N = 2$	$N = 5$	$N = 1$	$N = 2$	$N = 5$
\mathcal{M}^*	3.63 [3.57, 3.74]	2.56 [2.50, 2.75]	1.68 [1.59, 1.95]	—	—	—
\mathcal{M}_1	3.71 [3.63, 3.75]	2.86 [2.59, 3.21]	2.14 [1.82, 2.49]	.996	.989	≈ 1.0
\mathcal{M}_2	3.75 [3.66, 3.78]	2.75 [2.61, 2.90]	1.90 [1.77, 2.03]	.691	.903	≈ 1.0
\mathcal{M}_3	3.72 [3.69, 3.76]	2.77 [2.66, 3.14]	2.17 [2.00, 2.40]	.334	.612	≈ 1.0

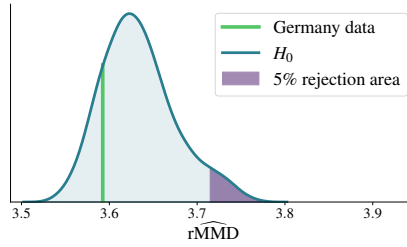


Figure I.5: Inverse multiquadratic kernel. Representation of the Germany COVID-19 time series with respect to the distribution of $\widehat{\text{rMMD}}$ under H_0 .

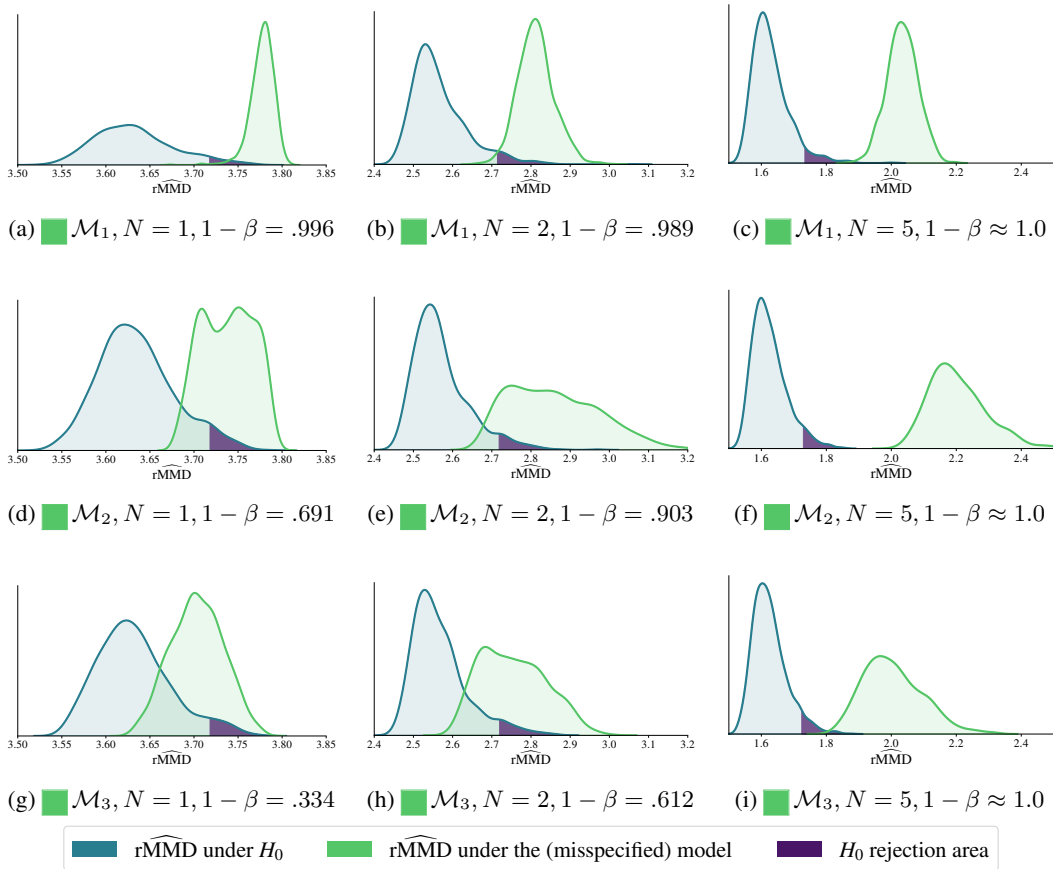


Figure I.6: Inverse multiquadratic kernel. Detailed illustration of the power analysis in **Experiment 2**